NeuroImage: Clinical 34 (2022) 102977

Contents lists available at ScienceDirect

NeuroImage: Clinical

journal homepage: www.elsevier.com/locate/ynicl

Disrupted coupling between salience network segregation and glucose metabolism is associated with cognitive decline in Alzheimer's disease – A simultaneous resting-state FDG-PET/fMRI study

Miao Zhang [a,1], Ziyun Guan [b,1], Yaoyu Zhang [b,1], Wanqing Sun [b], Wenli Li [b], Jialin Hu [b], Binyin Li [c], Guanyu Ye [c], Hongping Meng [a], Xinyun Huang [a], Xiaozhu Lin [a], Jin Wang [a], Jun Liu [c], Biao Li [a,d,*], Yao Li [b,*]

[a] Department of Nuclear Medicine, Ruijin Hospital, Shanghai Jiao Tong University School of Medicine, Shanghai 200025, China
[b] School of Biomedical Engineering, Shanghai Jiao Tong University, Shanghai 200030, China
[c] Department of Neurology & Institute of Neurology, Ruijin Hospital, Shanghai Jiao Tong University School of Medicine, Shanghai 200025, China
[d] Collaborative Innovation Center for Molecular Imaging of Precision Medicine, Ruijin Center, Shanghai 200025, China

ARTICLE INFO

Keywords:
Alzheimer's disease
Glucose metabolism
Hybrid PET/MR
Network segregation
Triple network model
Salience network

ABSTRACT

The aberrant organization and functioning of three core neurocognitive networks (NCNs), i.e., default-mode network (DMN), central executive network (CEN), and salience network (SN), are among the prominent features in Alzheimer's disease (AD). The dysregulation of both intra- and inter-network functional connectivities (FCs) of the three NCNs contributed to AD-related cognitive and behavioral abnormalities. Brain functional network segregation, integrating intra- and inter-network FCs, is essential for maintaining the energetic efficiency of brain metabolism. The association of brain functional network segregation, together with glucose metabolism, with age-related cognitive decline was recently shown. Yet how these joint functional-metabolic biomarkers relate to cognitive decline along with mild cognitive impairment (MCI) and AD remains to be elucidated. In this study, under the framework of the triple-network model, we performed a hybrid FDG-PET/fMRI study to evaluate the concurrent changes of resting-state brain intrinsic FCs and glucose metabolism of the three NCNs across cognitively normal (CN) (N = 24), MCI (N = 21), and AD (N = 21) groups. Lower network segregation and glucose metabolism were observed in all three NCNs in patients with AD. More interestingly, in the SN, the coupled relationship between network segregation and glucose metabolism existed in the CN group ($r = 0.523$, $p = 0.013$) and diminished in patients with MCI ($r = 0.431$, $p = 0.065$) and AD ($r = 0.079$, $p = 0.748$). Finally, the glucose metabolism of the DMN ($r = 0.380$, $p = 0.017$) and the network segregation of the SN ($r = 0.363$, $p = 0.023$) were significantly correlated with the general cognitive status of the patients. Our findings suggest that the impaired SN segregation and its uncoupled relationship with glucose metabolism contribute to the cognitive decline in AD.

1. Introduction

Large-scale network disruption of brain's functional organization has been identified to be associated with Alzheimer's disease (AD) progression (Brier et al., 2012). Among them, the aberrant organization and functioning of three core neurocognitive networks (NCNs), i.e., default-mode network (DMN), central executive network (CEN), and salience network (SN), are the prominent features (Agosta et al., 2012; Badhwar et al., 2017; Lim et al., 2014; Myers et al., 2014). For example, using functional magnetic resonance imaging (fMRI) technique, dysfunctions of the DMN have been consistently shown in patients with AD, which were closely related to their self-related episodic memory deficits (Contreras et al., 2019; Dai et al., 2019; Greicius et al., 2004; Jones et al., 2016; Scherr et al., 2021). Disruptions in the CEN and SN were also

* Corresponding authors at: Department of Nuclear Medicine, Ruijin Hospital, Shanghai Jiao Tong University School of Medicine, Shanghai 200025, China (B. Li). School of Biomedical Engineering, Shanghai Jiao Tong University, Shanghai 200030, China (Y. Li).
E-mail addresses: lb10363@rjh.com.cn (B. Li), yaoli@sjtu.edu.cn (Y. Li).
[1] These authors contributed equally to this work.

https://doi.org/10.1016/j.nicl.2022.102977
Received 24 September 2021; Received in revised form 26 February 2022; Accepted 28 February 2022
Available online 1 March 2022

found in patients with AD (Agosta et al., 2012; Zhao et al., 2019; Zhou et al., 2010), and dysfunction of the SN has been shown closely related to the cognitive decline in the aging adults (Onoda et al., 2012). A triple-network model, consisting of the DMN, CEN, and SN, has been proposed as an important framework for understanding the psychopathology across multiple brain disorders (Menon, 2011). Disruptions in the triple network model, including deficits in access, engagement, and disengagement of the three networks, have been shown to play a prominent role in AD. Alterations in both intrinsic (He et al., 2014; Jones et al., 2016; Zhao et al., 2019) and interactive (Chand et al., 2017; Li et al., 2019) functional activities of the three networks have been shown and associated with the cognitive dysfunctions of AD patients.

In the triple network model, the SN acts as an integral hub in mediating dynamic interactions between the DMN and CEN in response to general cognitive demands. While the DMN is actively engaged in internal mental events, the SN can initiate network switching to disengage the DMN and promote the CEN when detecting external salient events. Within the triple-network model, disruptions in one of the NCNs would impact the other two, leading to clinical manifestations beyond the primary deficits. Emerging evidence has shown that the interactions among the three core NCNs become an important aspect of understanding the cognitive dysfunctions in AD. Brier et al. (Brier et al., 2012) demonstrated a widespread loss of intra-network connectivity and inter-network anti-correlation with increased AD severity. More specifically, Chand et al. (Chand et al., 2017) reported that the triple-network model switched from an SN-modulated model in healthy elderly subjects to a CEN-modulated model in patients with mild cognitive impairment (MCI). Similarly, Li et al. (Li et al., 2019) found increased inter-network connectivity between SN and DMN or CEN in patients with MCI and AD, suggesting a disrupted SN-centered triple-network model. Nevertheless, the pathological mechanisms underlying the functional alterations of the triple-network along with AD progression remain to be elucidated.

In recent years, there has been increasing interest to explore the brain metabolic processes underlying the functional changes by a combined fMRI with PET imaging approach. Manza et al. (Manza et al., 2020) reported that the brain functional network segregation, together with glucose metabolism, decreased with aging and associated with age-related cognitive decline. The network segregation, as an integrative biomarker incorporating both intra- and inter-network FCs, is essential for the optimized "trade-off" between minimizing energy cost and maximizing functional efficiency in normal brain (Bullmore and Sporns, 2012; Wig, 2017). Lately, low segregation in episodic memory networks has been shown to be associated with AD pathology (Cassady et al., 2021). Moreover, Ewers et al. (Ewers et al., 2021) suggested that the global network segregation was associated with cognitive resilience in AD, while Arenaza-Urquijo et al. (Arenaza-Urquijo et al., 2019) demonstrated that FDG-PET could be a proxy of the cognitive resilience. These previous findings together shed light on the functional and metabolic mechanism as a potential neural basis of cognitive dysfunction in AD. Nevertheless, how the underlying relationship between network segregation and glucose metabolism is affected by AD has not been fully understood.

To better understand the concurrent changes of functional-metabolic signals within the triple-network and capture the cross-modal interactions, we performed a hybrid PET/MRI study to simultaneously evaluate resting-state brain intrinsic activity and glucose metabolism. The use of hybrid PET/MRI minimized the fluctuations in NCN functional or metabolic features due to different brain states or moods of the participants, thus ensuring more accurate evaluations of the concomitant changes of multimodal features (Harrison et al., 2008; Waites et al., 2005). For resting-state fMRI data, we used the intra- and inter-network functional connectivity strength (FCS), as well as brain network segregation, to evaluate the intrinsic functional connectivity features systematically. The regional glucose metabolism was measured using ^{18}F-FDG-PET in the same scan. We tested the following hypotheses: 1) brain network segregation in the triple-network model would be lower in patients with MCI and AD; 2) the association between brain network segregation and glucose metabolism would be disrupted in patients with AD, which would be related to the declines of cognitive functions in patients.

2. Materials and methods

2.1. Participants

A total of 70 subjects participated in our study, including 24 cognitively normal (CN) participants, 23 patients with MCI, and 23 patients with AD. The patients with MCI and AD were recruited from the Memory Clinic at Ruijin Hospital, Shanghai. The CN participants were recruited through local advertisements. Each participant was initially screened by the Mini-Mental State Examination (MMSE, Chinese Version) (Folstein et al., 1975), global clinical dementia rating (CDR $>$ 0.5 for AD diagnosis) (Morris, 1993), Zung Self-rating Anxiety Scale, Self-rating Depression Scale, and activity of daily living questionnaire. MCI and AD were diagnosed according to the National Institute on Aging-Alzheimer's Association (NIA-AA) workgroups (Albert et al., 2011; McKhann et al., 2011). All participants in the CN, MCI, and AD groups had CDR scores $=$ 0, 0.5, and $>$ 0.5, respectively. Exclusion criteria include: (1) psychiatric or other neurological diseases; (2) pregnancy or renal failure (critical for PET imaging); (3) major systemic disease; (4) history of traumatic brain injury; (5) drug or alcohol addiction. The study was approved by the Institutional Review Board of Ruijin Hospital and in accordance with the ethical standards of the Helsinki declaration and its later amendments or comparable ethical standards. Written informed consents were obtained from all participants or their designees.

2.2. Image acquisition

All imaging data were acquired on a 3T integrated Siemens Biograph mMR scanner (Siemens Healthcare, Erlangen, Germany) using a 12-channel phase-array head coil. During the scan, all participants were instructed to lie supine with eyes closed, without systematic thinking or falling asleep. Each subject was required to fast for at least 6 h before receiving a bolus injection of the fluorine ^{18}F-fluorodeoxyglucose (^{18}F-FDG) using a mean dose of 204.3 $\pm$ 34.6 MBq (range 140.6–329.3 MBq). Simultaneous PET/MR imaging was performed at 40 min after the injection. The ^{18}F-FDG-PET images were acquired in sinogram mode for 15 mins (127 slices; matrix size $=$ 344 $\times$ 344). The PET emission data were reconstructed using ordered subset expectation maximization algorithm (21 subsets, 4 iterations) and post-filtered with an isotropic 2 mm full-width half-maximum (FWHM) Gaussian kernel. The reconstructed PET image voxel size was 2.1 $\times$ 2.1 $\times$ 2.0 mm^3. Attenuation correction was performed based on the Dixon method with an additional model-based bone compartment to improve the accuracy of standard uptake value (SUV) estimation (Koesters et al., 2016). The T1-weighted MR images were obtained using the magnetization-prepared rapid acquisition gradient echo (MPRAGE) sequence: repetition time (TR) $=$ 1900 ms; echo time (TE) $=$ 2.44 ms; flip angle (FA) $=$ 9°; field of view (FOV) $=$ 256 mm; voxel size $=$ 0.5 $\times$ 0.5 $\times$ 1.0 mm^3; number of slices $=$ 192. Resting-state fMRI images were acquired using echo-planar imaging (EPI) sequence: TR $=$ 2000 ms; TE $=$ 22 ms; FA $=$ 90°; FOV $=$ 192 mm; voxel size $=$ 3.0 $\times$ 3.0 $\times$ 3.0 mm^3; number of slices $=$ 36; number of volumes $=$ 240.

2.3. FMRI data preprocessing

The fMRI data were preprocessed using the Analysis of Functional Neuroimaging (AFNI) software package (Cox, 1996). The first ten volumes of each subject were removed to reduce the effects of noises and artifacts introduced by magnetic field stabilization and subject

adaptation to the scanning. Slice timing and head motion corrections were performed. To exclude the possible effects of head motion, we performed a scrubbing procedure that the fMRI data volume was censored if its framewise displacement was > 0.5 mm (Power et al., 2012). In order to have sufficient time points for FC analysis, subjects with $< 75\%$ of data remaining after censoring were excluded from the analysis. Nonlinear spatial normalization to the Montreal Neurological Institute (MNI) space was applied to each image, with a resampled isotropic spatial resolution of 3 mm. Temporal band-pass filtering (0.01–0.1 Hz) was performed to reduce the low-frequency drifts and high-frequency physiological noises. The nuisance signals were regressed out from each time course, including six head motion parameters and their first derivatives, averaged signals from white matter, cerebral spinal fluid, and the global signal. Preprocessing of the fMRI images without global signal regression was also performed to demonstrate that it did not exert a significant effect on our main findings (see Fig.A.1 in Appendix A). Finally, spatial smoothing was performed using a 6 mm FWHM Gaussian kernel.

2.4. PET data processing

The FDG-PET data were processed using the statistical parametric mapping software (SPM12). For each subject, the PET data were registered to the corresponding T1-weighted images using affine transformation, followed by partial volume correction using the Müller-Gärtner method (Müller-Gärtner et al., 1992) with the PETPVE12 toolbox (Gonzalez-Escamilla et al., 2017). After that, the T1-weighted images were spatially normalized to the MNI 152 template using the DARTEL algorithm. The FDG-PET images were warped to the standard MNI space using the same transformation parameters applied for T1 image normalization and smoothed using a 6 mm FWHM Gaussian kernel. Finally, the ^{18}F-FDG-PET standardized uptake value ratio (SUVR) values were calculated using the mean uptake of cerebellar gray matter as the reference, because the cerebellum is considered one of the least affected regions in AD (Benson et al., 1983; Minoshima et al., 1997). For the FDG analysis, the functional network masks obtained from the fMRI analyses were used. Regional glucose metabolism was calculated as the mean SUVR within the network mask.

2.5. Functional brain network parcellation

The functional brain network parcellation was performed using the data of the CN group. The robustness of the parcellation was validated by using the data of the MCI and AD groups (see Fig.A.2 in Appendix A). For each subject, Pearson's correlation coefficients, r, were calculated between the time courses of each pair of voxels within the group-averaged grey matter mask, leading to an $N \times N$ whole brain connectivity matrix, where N is the number of gray matter voxels. Following the previous literature (Liang et al., 2015), the negative correlations were set to zero, and our analysis considered the positive correlations only. To remove the weak correlations that might arise from signal noises, a binary connectivity matrix was created with the data assigned to 1 if $r > 0.25$ and 0 otherwise (Liang et al., 2013). We also tried thresholds with $r > 0.2$ and $r > 0.3$ for the parcellation, and compared the network segregation based on these two thresholds between groups. Similar results were shown as using $r > 0.25$ (see Table A.1 and Fig.A.3 in Appendix A). Group-averaged sparse matrix was generated by discarding the connections present in less than half of the subjects. A random-walk-based Infomap algorithm was applied for the network parcellation, which showed its superiority in handling large networks and stability in complex conditions (Rosvall and Bergstrom, 2008). The Infomap algorithm transforms finding the network structure into an encoding problem. It seeks a network partition to minimize the length of description of random walk process on the network. The Infomap algorithm is based on Huffman coding, and further divides the network into two levels of description, i.e., coding for clusters and nodes within clusters, respectively (Rosvall and Bergstrom, 2008). Subgraph assignments for each node were returned as numbers.

The modularity parameter Q is a whole-graph measure evaluating if the whole-brain can be well organized into discrete networks (Newman and Girvan, 2004). We used modularity Q as a quality-check for the parcellation achieved by Infomap algorithm to make sure the parcellation was reasonable. The modularity Q was defined as:

$$Q = \frac{1}{L}\sum_{i,j\in N}[w_{ij} - \frac{k_i k_j}{L}]\delta_{m_i,m_j}$$

where i and j represent two individual nodes; L is the number of all edges in the network; $w_{i,j}$ denotes the connectivity between nodes i and j; k_i and k_j are the number of edges linked to node i and j; m_i and m_j denote the modules where nodes i and j belong to; and δ is the Kronecker delta function. A network with a strong modular structure typically has a modularity Q ranged from 0.3 to 0.7 (Newman and Girvan, 2004). In our study, Q was equal to 0.61.

2.6. Intra- and inter-network functional connectivities

In the following network analyses of the intra- and inter-network functional connectivities, as well as network segregation, we exclusively focused on the three networks (i.e., the DMN, CEN and SN) to test our hypotheses on the AD-related functional and metabolic alterations under the framework of the triple network model. The selections of the networks of interest from the whole-brain parcellation result were based on visual inspection according to previous literatures.

The intra-network functional connectivity (intra-FC) was evaluated by FCS (Liang et al., 2013; Zhang et al., 2021a). The mean FCS of a given network module s was denoted as C_s, which was calculated as:

$$C_s = \frac{\sum_{i,j\in s} z_{i,j}}{N_s \times (N_s - 1)}$$

where N_s is the number of voxels within module s; and $z_{i,j}$ denotes the Fisher's z-transformed correlation coefficient r between voxel i an j within module s.

The inter-network functional connectivity (inter-FC) was used to evaluate functional connectivity between network s and t, which was defined as:

$$C_{s,t} = \frac{\sum_{i\in s,j\in t} z_{i,j}}{N_s \times N_t}$$

where N_s is the number of voxels within module s; N_t is the number of voxels within module t; and $z_{i,j}$ denotes the Fisher's z-transformed correlation coefficient r between voxel i within module s and voxel j within module t.

Based on the interesting results we obtained on the inter-FC between the DMN and SN/CEN (described in the Result section), we additionally investigated the inter-FC changes between the DMN and other non-associative networks, including the visual and somatomotor networks.

2.7. Network segregation

The network segregation (Chan et al., 2014) was calculated among three core NCNs. It was measured by integrating intra- and inter-FCs for a given network, which was defined as:

$$\text{Segregation} = \frac{\overline{Z}_w - \overline{Z}_b}{\overline{Z}_w}$$

where $\overline{Z}_w$ is the mean of Fisher's z-transformed r between voxels within the same network; and $\overline{Z}_b$ is the mean Fisher's z-transformed r between voxels of one network to voxels in all the other networks. Weak correlations ($r < 0.25$) that might arise from signal noises were excluded in all

analyses (Liang et al., 2013).

2.8. Statistical analysis

All the statistical analyses were carried out using SPSS software (version 25, IBM Corporation, Armonk, NY, USA). Normality tests were performed for all continuous variables using the Kolmogorov-Smirnov test. The demographics and clinical characteristics were compared among the three groups using chi-squared tests for the categorical measures and one-way analyses of variance (ANOVA) for the other variables.

To determine whether there are differences in the intra-FC, inter-FC, network segregation, and FDG-SUVR among the CN, MCI, and AD groups, we performed one-way analysis of covariance (ANCOVA) with age and sex as covariates, followed by post hoc two-sample t-tests. Multiple comparisons were corrected using Bonferroni correction with an alpha threshold of 0.004 (i.e., 0.05/12, 4 imaging markers in 3 functional networks) as statistically significant. In addition, the relationships between functional connectivity and glucose metabolism were explored using Pearson's or Spearman's partial correlation analyses depending on the normality of the data, with age and sex as covariates. Spearman's partial correlation analyses were used to explore the associations of intra-FC, inter-FC, network segregation and FDG-SUVR of the three networks with MMSE scores, with age and sex as covariates. For all partial correlation analyses, $p < 0.05$ was considered as statistically significant.

3. Results

3.1. Demographic and clinical characteristics

After image quality control, 24 CN controls, 21 patients with MCI and 21 patients with AD were included for data analysis. Their demographics and clinical information are listed in Table 1. No significant differences were found in age, sex, or education among the three groups. On average, the patients were mild to moderately impaired with the general cognitive function (MCI: mean MMSE score of 27.33, range from 24 to 30; AD: mean MMSE score of 20.38, range from 4 to 27). The patients with AD had significantly lower MMSE scores compared to the CN and MCI groups ($p < 0.001$), so did the patients with MCI compared to the CN group ($p = 0.041$).

3.2. Parcellation of the three core neurocognitive networks

The parcellation results of the three core NCNs (i.e., the DMN, CEN, and SN) are shown in Fig. 1a. We also performed functional brain network parcellation on the MCI and AD groups and obtained similar results (see Fig.A.2 in Appendix A). The DMN was composed of medial prefrontal cortex, posterior cingulate cortex and precuneus, bilateral middle temporal gyrus and bilateral angular gyrus. The CEN was composed of bilateral dorsolateral prefrontal cortex and bilateral posterior parietal cortex. The SN was composed of dorsal anterior cingulate cortex and bilateral insula. The regions included in the three networks were consistent with previous literature (see Table A.2 in Appendix A). The group-averaged FCS and FDG-SUVR maps within the triple-network region are illustrated in Fig. 1b and Fig. 1c, respectively. Lower FCS and FDG in MCI and AD can be observed by visual inspection.

Table 1
Demographic and clinical data.

	CN	MCI	AD	p value
Sample size	24	21	21	
Age, years	66.9(8.0)	70.6(8.6)	66.3(9.4)	0.23
Sex, Female/Male	13/11	13/8	15/6	0.49
Education, years	13.6(2.2)	12.8(3.7)	11.9(3.7)	0.21
MMSE	29.5(0.7)	27.3(1.6)[a]	20.4(5.9)[b,c]	< 0.001
CDR 0/0.5/1/2	24/0/0/0	0/21/0/0	0/0/16/5	

Note: Data are presented as mean (SD). Chi-square was used for sex comparisons, one-way ANOVA with post-hoc two-sample *t*-test was used for comparisons of age, education and MMSE scores among all groups.
Abbreviations: CN, cognitively normal controls; MCI, mild cognitive impairment; AD, Alzheimer's Disease; MMSE, Mini-Mental State Examination; CDR, Clinical Dementia Rating.
[a] CN ≠ MCI ($p < 0.05$); [b] MCI ≠ AD ($p < 0.05$); [c] CN ≠ AD ($p < 0.05$).

3.3. Altered intra- and inter-network functional connectivity among the three groups

Fig. 2a shows the group averaged intra- and inter-network functional connectivity matrices of DMN, CEN, and SN for the three groups. The between-group comparison results are illustrated in Fig. 2b and 2c. For DMN and CEN, weaker intra-FCs were observed in the AD group compared to the CN group (DMN: $p = 0.032$; CEN: $p = 0.016$). However, no significant difference was observed in the intra-FC of the SN among the three groups. Furthermore, higher inter-FC between the DMN and SN was found in the AD group compared to the CN group ($p = 0.016$). In the analysis of the non-associative networks, we found higher inter-FCs between the DMN and the visual network ($p = 0.042$), as well as between the DMN and the somatomotor network ($p = 0.036$) in the AD group compared to the CN group, respectively (see Fig. A.4 in Appendix A).

3.4. Lower network segregation and glucose metabolism in triple networks

The voxel-wise FC matrices of the three NCNs are shown in Fig. 3a. Trends of lower network segregations were observed for all three functional networks in patients with AD. As displayed in Fig. 3b, lower network segregations of the DMN ($p = 0.006$), CEN ($p = 0.002$) and SN ($p = 0.017$) were observed in patients with AD compared to the CN group. Besides, lower network segregation of the CEN was also found in AD compared to MCI patients ($p = 0.032$). Glucose metabolism, estimated by FDG-SUVR, exhibited a similar pattern (see Fig. 3c). Hypometabolism of the three NCNs were shown in the AD group compared to the CN group (DMN: $p < 0.001$; CEN: $p < 0.001$; SN: $p = 0.008$) and MCI group (DMN: $p = 0.007$; CEN: $p = 0.009$).

3.5. Disrupted segregation-metabolism coupling

Fig. 4 and Table 2 show the correlation results between network segregation and glucose metabolism for the three NCNs. In the SN, the positive correlation between network segregation and glucose metabolism in the CN group ($r = 0.523$, $p = 0.013$) diminished in the MCI ($r = 0.431$, $p = 0.065$) and AD ($r = 0.079$, $p = 0.748$) groups. In the DMN and CEN, no significant correlation between network segregation and glucose metabolism was observed in any group (see Table 2).

3.6. Correlations between imaging parameters and the MMSE scores

As illustrated in Fig. 5a and 5b, both glucose metabolism of the DMN ($r = 0.380$, $p = 0.017$) and network segregation of the SN ($r = 0.363$, $p = 0.023$) decreased with reduced MMSE scores in the combined MCI and AD group.

4. Discussion

4.1. Lower segregation of triple-network model in AD

Aberrant organization and functioning of the three core NCNs, i.e., DMN, CEN and SN, have been commonly identified in a variety of neurological and psychiatric disorders (Menon, 2011). The DMN has been typically associated with self-referential process and episodic memory, of which the disruptions are the most common presenting

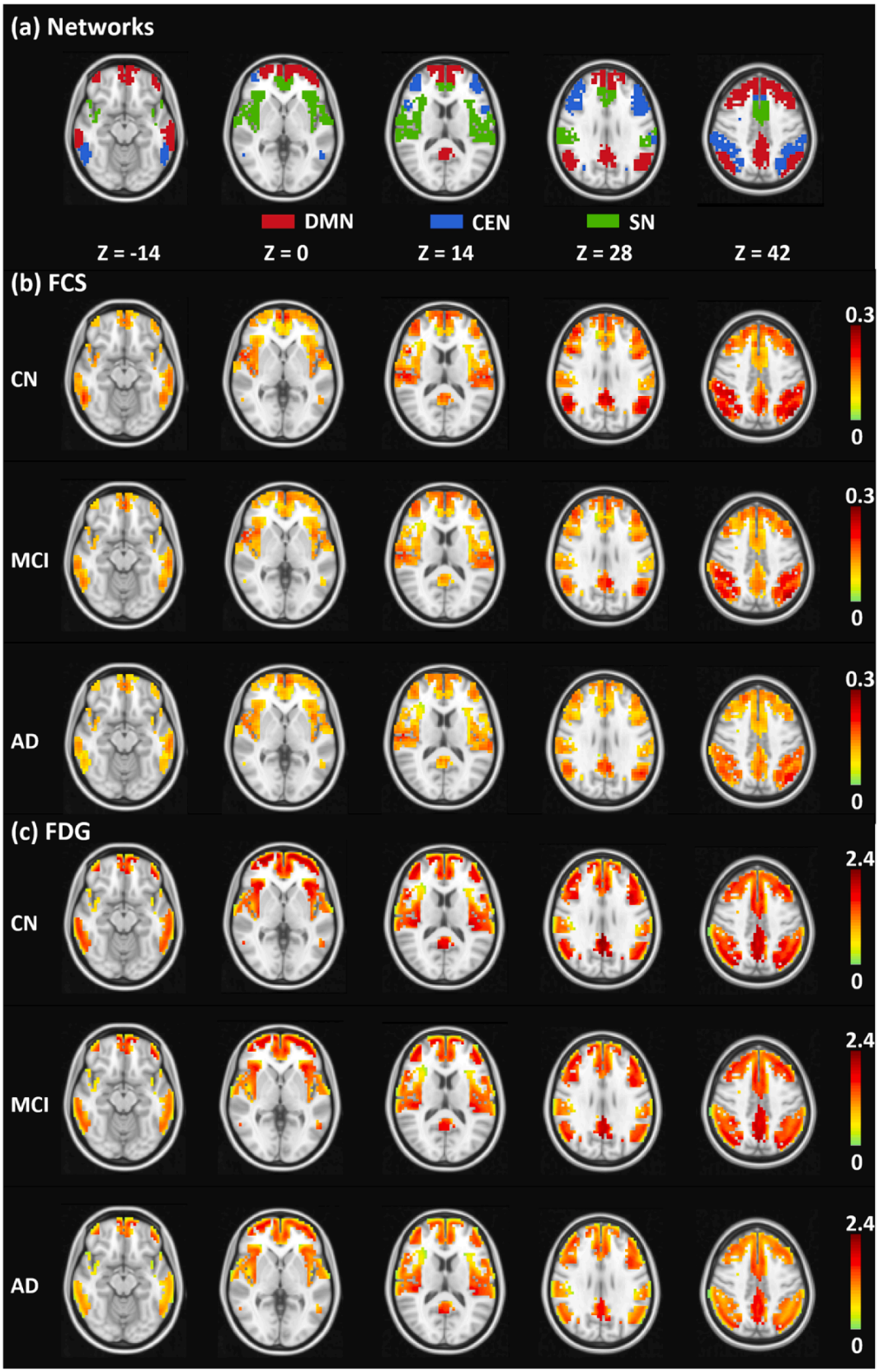

Fig. 1. The parcellation results of triple networks and the maps of average FCS and FDG in the CN, MCI, and AD groups. **(a)** Illustrations of the parcellation results for the DMN (red), CEN (blue) and SN (green) using fMRI data. The average FCS **(b)** and FDG-SUVR **(c)** maps of the CN, MCI, and AD groups, respectively. The FCS and FDG-SUVR maps are masked by the triple-network parcellation results in (a). All the maps are overlaid on the MNI T1-weighted template. Abbreviations: DMN, default-mode network; CEN, central executive network; SN, salience network; FCS, functional connectivity strength; FDG, fluorodeoxyglucose; CN, cognitively normal controls; MCI, mild cognitive impairment; AD, Alzheimer's Disease. (For interpretation of the references to colour in this figure legend, the reader is referred to the web version of this article.)

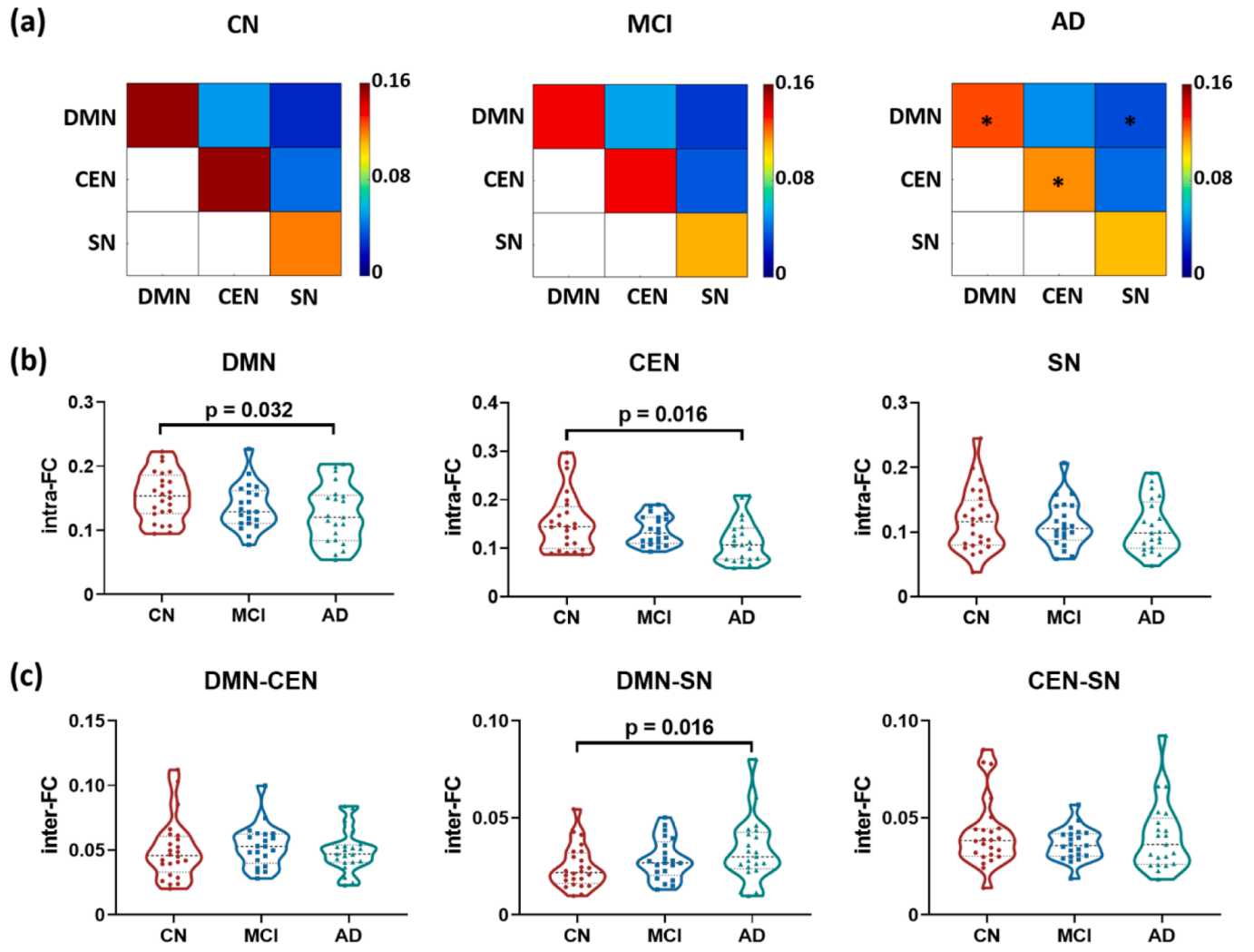

Fig. 2. Intra- and inter-network functional connectivities of the DMN, CEN and SN in the CN, MCI, and AD groups. **(a)** Functional connectivity matrices demonstrating the intra- and inter-FCs of the triple networks. *p_uncorrected < 0.05. **(b)** Changes of intra-FC of the triple networks in MCI and AD groups. Lower intra-FC were found in the DMN and CEN of patients with AD compared to the CN group. **(c)** Changes of inter-FC of the triple network in MCI and AD groups. Higher inter-FC between the DMN and SN was found in patients with AD compared to the CN group. Group differences were compared via GLM analysis with post-hoc two-sample t-tests. Age and sex were included as covariates. Abbreviations: DMN, default-mode network; CEN, central executive network; SN, salience network; FC, functional connectivity; CN, cognitively normal controls; MCI, mild cognitive impairment; AD, Alzheimer's Disease.

symptoms of AD (McKhann et al., 2011). It is also the first brain functional network identified to be affected by AD (Greicius et al., 2004) and has been henceforth extensively studied. The CEN is crucial for multiple higher-order cognitive functions such as working-memory, problem-solving, and decision-making (Menon, 2011). Reduced FC in the CEN-related regions, i.e., bilateral inferior parietal lobe, superior parietal lobe, inferior frontal gyrus and left middle frontal gyrus, were consistently found in AD or individuals with amyloid-β (Aβ) deposition (Dai et al., 2015; Li et al., 2019; Lim et al., 2014). Our findings of weaker intra-network FCs of DMN and CEN in patients with AD agreed with the majority of the studies. A common hypothesis about this is that the hub regions within DMN and CEN are preferentially targeted by AD-related pathological processes, including Aβ deposition (Dai et al., 2015).

The SN is involved in detection of salient events and generation of appropriate behavioral responses to salient stimuli. In the triple network model, the SN plays a crucial role for initiating network switching, which led to the engagement of the CEN and the disengagement of the DMN in task-related events (Menon, 2011; Sridharan et al., 2008). Disrupted connectivity within the SN in AD were reported in previous studies, showing heterogeneous patterns among different subregions (Brier et al., 2012; Chen et al., 2013). While Balthazar et al. reported increased FC in anterior SN, decreased FC in bilateral frontoinsular cortex were found in other studies for patients with AD compared to CNs (Balthazar et al., 2014; Dai et al., 2015; He et al., 2014). This heterogeneity in the FC of subregions within the SN might explain the non-significant difference in the whole SN FCS among the three groups in our study. Following this line of thought, we explored the Intra-FC in subregions of the SN parcellated using the Infomap algorithm. As displayed in Fig.A.5 and Table.A.3 in Appendix A, we found a significant decrease in the left posterior insula ($p = 0.037$). Although we could not find many other significant differences in the subnetworks, which might be due to the limited sample size, it is interesting to find that the patterns of changes were different within different subsystems, e.g., increase in FCS of left ventral anterior insula and decreases in FCS of multiple subregions of insula in the AD group. Therefore, further studies exploring the heterogeneous functional and metabolic changes in the subsystems of the current triple-network framework are in merit. In addition, the preservation of the FC in SN compared to DMN and CEN might also be explained by the graded network degeneration hypothesis that Aβ-related damages to the intrinsic connectivity first started in the DMN and followed by other networks with the development of AD (Myers et al., 2014). Interestingly, we observed a higher SN-DMN

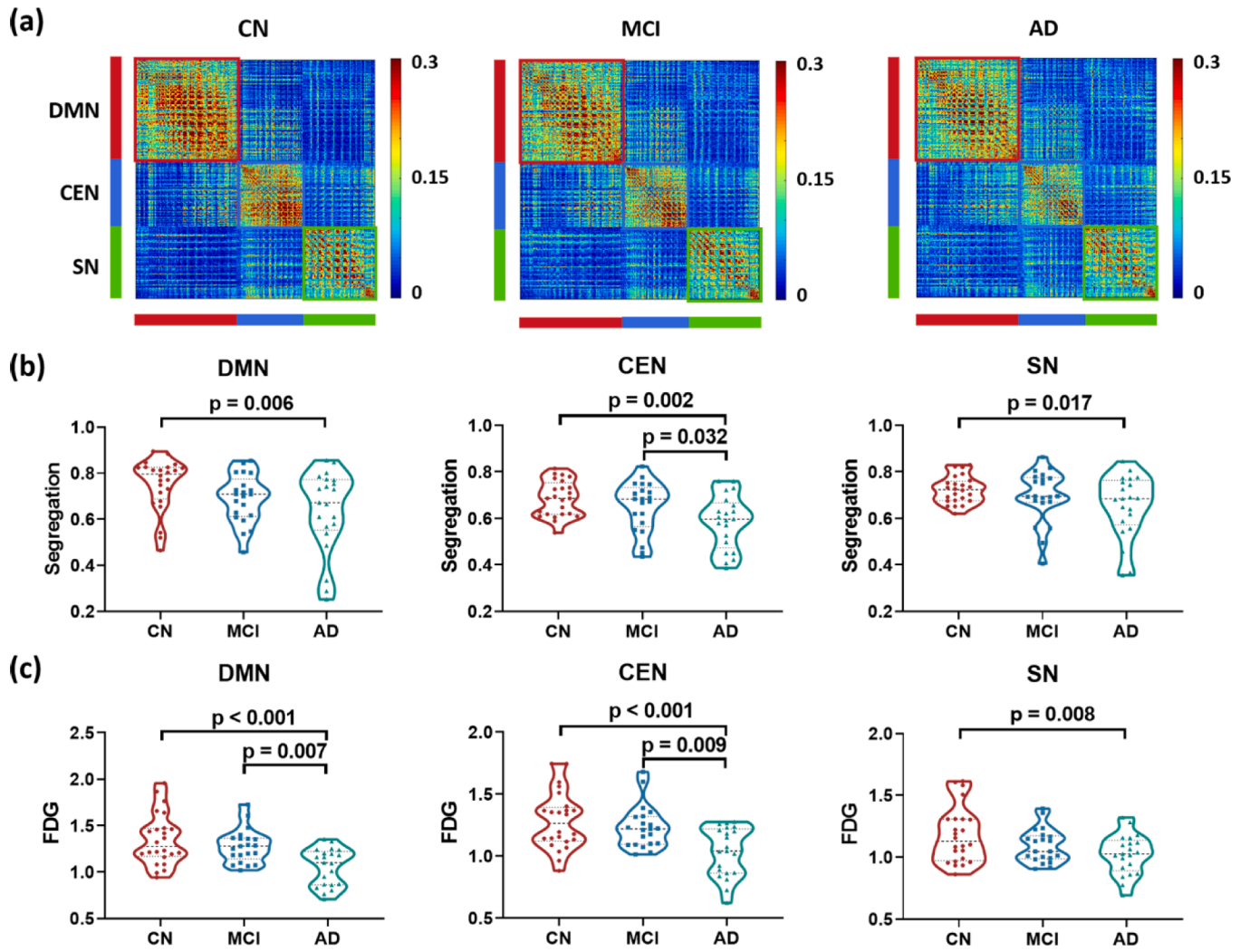

Fig. 3. Network segregation and glucose metabolism of the DMN, CEN and SN in the CN, MCI, and AD groups. **(a)** Voxel-wise functional connectivity matrices for the triple networks in the three groups. **(b)** Changes of network segregation of the triple network in MCI and AD. Lower network segregations were observed in patients with AD compared to the CN group in all three functional networks, and in patients with AD compared to patients with MCI in the CEN. **(c)** Changes of FDG-SUVR of the triple network in MCI and AD. For DMN and CEN, hypometabolism were observed in patients with AD compared to the other two groups. In the SN, hypometabolism were observed in patients with AD compared to the CN group. Group differences were compared via GLM analysis with post-hoc two-sample t-tests. Age and sex were included as covariates. Abbreviations: DMN, default-mode network; CEN, central executive network; SN, salience network; FDG, fluorodeoxyglucose; CN, cognitively normal controls; MCI, mild cognitive impairment; AD, Alzheimer's Disease.

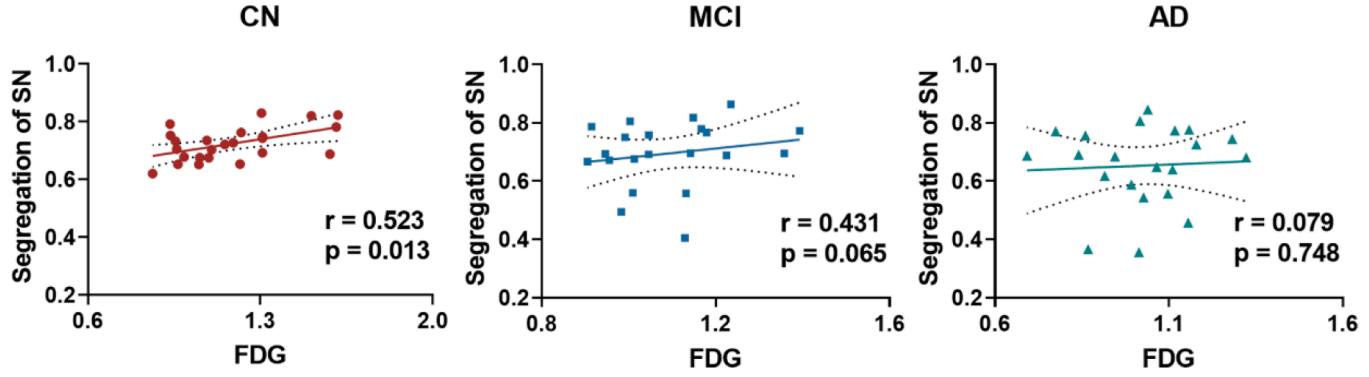

Fig. 4. Correlations between network segregation and FDG-SUVR in the SN of CN, MCI, and AD groups, respectively. A significant positive correlation between network segregation and FDG-SUVR was observed in CN group but not in the MCI or AD group. All partial correlation analyses were performed with age and sex as covariates. Abbreviations: SN, salience network; FDG, fluorodeoxyglucose; CN, cognitively normal controls; MCI, mild cognitive impairment; AD, Alzheimer's Disease.

Table 2
Partial correlations between network segregation and FDG in the triple networks.

Group	DMN		CEN		SN	
	r	p	r	p	r	p
CN	−0.053	0.815	0.155	0.491	**0.523**	**0.013**
MCI	0.058	0.813	0.134	0.584	0.431	0.065
AD	0.116	0.636	0.242	0.318	0.079	0.748

Partial correlation analyses were performed with age and sex as covariates.
Abbreviations: DMN, default mode network; CEN, central executive network; SN, salience network; CN, cognitively normal controls; MCI, mild cognitive impairment; AD, Alzheimer's Disease.

connectivity in patients with AD compared to the CN group, in line with a previous study (Li et al., 2019). This finding might indicate an impairment in the traditional SN-centered triple-network model with an inefficient regulation of SN to DMN activities in AD. In support of this, Chand et al. demonstrated a shift to the CEN-centered triple-network model in patients with MCI from the SN-centered one in the CN group (Chand et al., 2017). Although our work is mainly focused on the triple-network model in AD, it will be of great interest to further explore the inter-FC changes between the DMN and other networks. For example, we found increased inter-FCs between the DMN and the visual network, as well as between the DMN and the somatomotor network in the AD group compared to the CN group. Future work could be expanded to those non-associative networks to understand the functional-metabolic changes within large-scale systems of the brain in AD.

To further explore the alterations of intra- and inter-network connectivity in an integrated way, we compared the network segregation across the three groups for each network. In the triple-network model, we observed lower network segregations in all three networks of patients with AD compared to CNs and decreased segregation of CEN from MCI to AD groups. Our results agree with previous findings. Following the similar approach of segregation calculation as in our work, recent studies showed significant reduced segregations in the global system and the episodic memory networks in patients with AD (Cassady et al., 2021; Ewers et al., 2021). Using various other measures of segregation such as clustering coefficient or within-module degree, decreased segregation has been reported in the whole brain and multiple networks in patients with MCI and AD (Brier et al., 2014; Contreras et al., 2019; Costumero et al., 2020; Dai et al., 2019; Ng et al., 2021; Tumati et al., 2020). Together, these results indicate that the distinct and functionally specialized role of individual network seemed to be blurred in the brain functional organization of MCI and AD.

4.2. Association between triple-network segregation and glucose metabolism

Interestingly, we observed significant correlations between network segregation and glucose metabolism in the SN of the CN group. The relationship between brain glucose uptake and functional activity in the healthy population has been actively explored recently using combined fMRI and FDG-PET imaging. Associations of functional connectivity and glucose metabolism were found locally across different brain regions and brain states (Passow et al., 2015; Riedl et al., 2014; Tomasi et al., 2013). Furthermore, some discrepancies among brain regions can be largely explained by the spatially or network-wisely heterogeneous coupling relationships between glucose metabolism and functional connectivity, which are related with their function specializations (Shokri-Kojori et al., 2019). Manza et al. (Manza et al., 2020) found that both network segregation and glucose metabolism were negatively correlated with age in healthy adults in the association networks, which contained the three NCNs in our work. This indicated a possibly synchronized decline of both brain measures along with aging in the functional networks with relatively lower segregation property. However, they did not find a significant correlation between network segregation and glucose metabolism in the sensorimotor or the association network. The association network is a widespread brain region which covers the default-mode, frontoparietal, attention, cinguloopercular and salience networks. Thus the sensitivity to detect the variations within such a broad network might be reduced. This may explain the discrepancy between their results and ours. Nevertheless, they commented on the rationality of a theoretical association between the two measures, that the segregated organization of the brain minimizing the "wiring cost" might be related to energetics such as glucose metabolism. In support of this, they found accelerated age-related decline of glucose metabolism in brain networks with lower segregation such as SN, indicating the likely intrinsic linkage between the two measures (Manza et al., 2020). Our results show a coupled relationship between network segregation and glucose metabolism in SN, using a simultaneous PET-rsfMRI acquisition, which directly captured the inherent correlations between functional and metabolic signals in the brain. Our findings demonstrate the existence of such an intrinsic functional-metabolic linkage in the relatively lower segregated networks in the triple-network model.

It is noteworthy that using a recently developed functional PET (fPET) approach, Jamadar et al. (Jamadar et al., 2021) showed that fPET metabolic connectivity had a moderate similarity with functional connectivity and little similarity with static PET (sPET) metabolic connectivity in selected regions. It's proposed that the sPET metabolic connectivity measured the across-subject metabolic covariance and

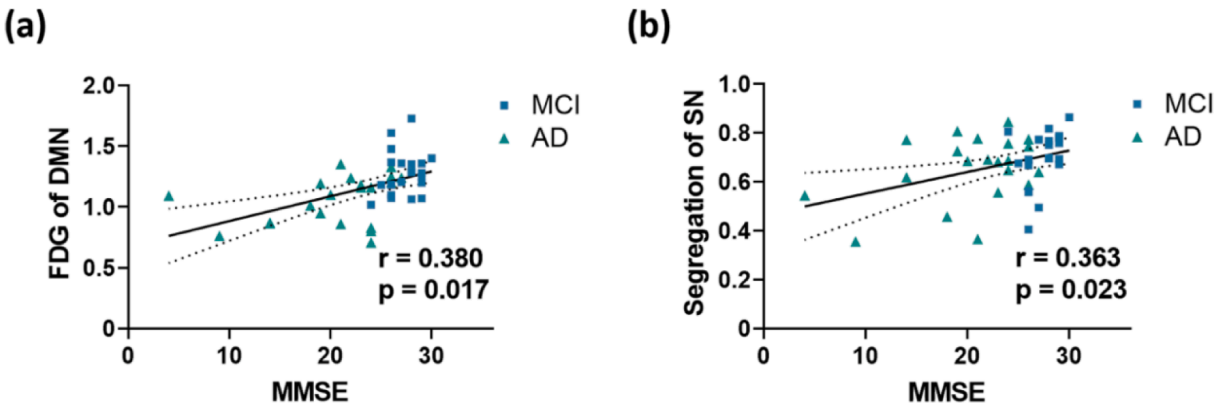

Fig. 5. Correlations between imaging biomarkers and MMSE scores of patients (combined MCI and AD groups). **(a)** The FDG-SUVR of DMN was positively correlated with MMSE scores. **(b)** The network segregation of SN was positively correlated with MMSE scores. All partial correlation analyses were performed with age and sex as covariates. Abbreviations: DMN, default-mode network; SN, salience network; FDG, fluorodeoxyglucose; MCI, mild cognitive impairment; AD, Alzheimer's Disease; MMSE, Mini-Mental State Examination.

could not be used to infer individual brain connectivity. In line with this, Ripp et al. (Ripp et al., 2020) found low or absent correlations between functional connectivity and sPET metabolic connectivity measured in large-scale NCNs. In this study, we used average FDG-SUVR, instead of fPET metabolic connectivity, to reflect the level of glucose consumption individually. Further studies exploring the relationship between fPET and FC biomarkers might improve our understanding about the functional-metabolic dynamics in relation to AD pathology.

4.3. Disrupted coupling of network segregation with glucose metabolism in AD

In our study, lower glucose metabolism in patients with AD compared to the CN and MCI groups were found in all three NCNs, in consistence with previous findings (Del Sole et al., 2008; Herholz et al., 2007; Marchitelli et al., 2018). A striking finding of our work is the diminished couplings between network segregation and glucose metabolism in patients with MCI and AD for SN. Similarly, disappeared correlations between surrogates of neural activity and metabolism (i.e., cerebral blood flow vs. cerebral metabolic rate of oxygen) with the progression of AD have been revealed in previous studies (Liu et al., 2014; Zhang et al., 2021b). The "small-world" organization of the human brain, characterized by segregated networks with strong intra-network connections and weaker inter-network connections, is essential for maintaining the energetic efficiency of brain metabolism (Manza et al., 2020). The dedifferentiation among functional networks might break the optimized "trade-off" between minimizing wiring costs and maximizing functional efficiency in the brain system (Bullmore and Sporns, 2012; Wig, 2017). Loss of network segregation may be a consequence of metabolic damages to the hub regions (Gratton et al., 2012; Mutlu et al., 2017; Wig, 2017), or a cause of the altered rates of hypometabolic progression (Franzmeier et al., 2017; Manza et al., 2020). Recent studies have suggested that AD could be associated with a metabolic shift from oxidative phosphorylation to aerobic glycolysis, which could jeopardize the original relationship between glucose utilization and functional activity (Atlante et al., 2017). Therefore, we speculate that while the network segregation is important for the brain energy-function trade-off, loss of the segregation or lower glucose metabolism during the development of AD could interrupt this balanced relationship.

In this study, the use of simultaneous FDG-PET/fMRI is of particular importance in uncovering the disrupted functional-metabolic relationship in relation to AD pathology. As the mental states may change on the scale of minutes, and the physiologic and metabolic status can vary on the scale of seconds (Heiss, 2016), synergistic measurements of FDG-SUVR and network segregation could truly reflect their correlations without confounds of intra-subject variations of physiologic and cognitive conditions. In addition, whereas BOLD-fMRI has relatively high spatial and temporal resolutions, FDG-PET is tightly connected to neural activity. Concurrent collections of the two measures can provide complementary information in understanding the energetics in AD. In this regard, our results showed the presence of a close relationship between glucose utilization and network segregation of the SN in the CN group, which diminished in the MCI and AD groups, suggesting that hypometabolism is in some way linked to a breakdown of the energy cost-efficiency trade-off affected by underlying pathological processes due to AD. Finally, the simultaneous imaging scheme improves patient comfortness and anatomical co-registration (Chen et al., 2018).

4.4. Disrupted network segregation in salience network associated with cognitive decline in AD

Finally, a significant positive correlation between the segregation of the SN and the MMSE score of patients with AD was shown in our study, indicating the detrimental effect on cognitive decline due to loss of segregation in it. The SN is composed of several subregions crucial for cognitive and neuropsychiatric behaviors. For instance, the anterior cingulate cortex (ACC) is associated with episodic motivation and directs selection of behavior (Egner, 2009); and the frontoinsular cortex is responsible for identifying salient stimuli from different types of sensory modalities (Cauda et al., 2011). Dysfunction of the property of detecting salient events for SN may cause failures in the appropriate assignment of saliency to external stimuli or internal mental events, leading to impaired cognitive/behavioral functions. Balthazar et al. found significant correlations between hyperactivity syndrome and the intrinsic FCs of the right ACC and right insula in patients with AD (Balthazar et al., 2014). He et al. demonstrated that the intrinsic FCs of the left frontoinsular cortex was correlated with the MMSE scores in patients with MCI and AD (He et al., 2014).

In addition to its specialized roles of higher-order cognitive functions, the SN has been suggested to play a critical role in the triple network model responsible for the control of DMN and CEN in reaction to salient stimuli (Balthazar et al., 2014). This capacity of switching between DMN and CEN could be harmed during AD progression, which would also lead to cognitive decline (He et al., 2014). Previous studies have shown that the unusually strengthened SN-related between-network interactions (Li et al., 2019) or decreased SN-DMN anti-correlations were associated with the MMSE scores (He et al., 2014). The cognitive impairment was associated with system-level disruption of brain regions including impaired balance of intra- and inter-communications (Chan et al., 2014). Ewers et al. showed that the segregation of brain functional networks was associated with cognitive resilience, which is an important modulating factor of cognitive decline in AD (Ewers et al., 2021). Since the SN plays not only specialized roles of several higher-cognitive functions but also a mediating role in the triple network model, its level of segregation combining the internal and external FCs provides a more sensitive biomarker to the overall cognitive performance in AD.

Funding

This work was supported by National Natural Science Foundation of China (81871083); Shanghai Jiao Tong University Scientific and Technological Innovation Funds (2019QYA12); Key Program of Multidisciplinary Cross Research Foundation of Shanghai Jiao Tong University (YG2021ZD28, YG2021QN40, and YG2022QN035); Shanghai Municipal Key Clinical Specialty (shslczdzk03403); and New Faculty Start-up Foundation of Shanghai Jiao Tong University (21X010500734).

CRediT authorship contribution statement

Miao Zhang: Conceptualization, Resources, Data curation, Investigation, Project administration, Funding acquisition. **Ziyun Guan:** Methodology, Software, Formal analysis, Writing – original draft, Visualization. **Yaoyu Zhang:** Methodology, Formal analysis, Writing – original draft, Writing – review & editing, Funding acquisition. **Wanqing Sun:** Software, Formal analysis. **Wenli Li:** Software, Formal analysis. **Jialin Hu:** Software, Formal analysis. **Binyin Li:** Data curation, Investigation. **Guanyu Ye:** Resources, Investigation. **Hongping Meng:** Data curation, Investigation. **Xinyun Huang:** Data curation, Investigation. **Xiaozhu Lin:** Data curation, Investigation. **Jin Wang:** Data curation, Investigation. **Jun Liu:** Resources, Data curation, Investigation. **Biao Li:** Conceptualization, Resources, Project administration, Supervision. **Yao Li:** Conceptualization, Methodology, Writing – original draft, Writing – review & editing, Supervision, Funding acquisition.

Declaration of Competing Interest

The authors declare that they have no known competing financial interests or personal relationships that could have appeared to influence the work reported in this paper.

Appendix A. Supplementary data

Supplementary data to this article can be found online at https://doi.org/10.1016/j.nicl.2022.102977.

References

Agosta, F., Pievani, M., Geroldi, C., Copetti, M., Frisoni, G.B., Filippi, M., 2012. Resting state fMRI in Alzheimer's disease: beyond the default mode network. Neurobiol. Aging 33 (8), 1564–1578. https://doi.org/10.1016/j.neurobiolaging.2011.06.007.

Albert, M.S., DeKosky, S.T., Dickson, D., Dubois, B., Feldman, H.H., Fox, N.C., Gamst, A., Holtzman, D.M., Jagust, W.J., Petersen, R.C., Snyder, P.J., Carrillo, M.C., Thies, B., Phelps, C.H., 2011. The diagnosis of mild cognitive impairment due to Alzheimer's disease: recommendations from the National Institute on Aging-Alzheimer's Association workgroups on diagnostic guidelines for Alzheimer's disease. Alzheimers Dement 7 (3), 270–279. https://doi.org/10.1016/j.jalz.2011.03.008.

Arenaza-Urquijo, E.M., Przybelski, S.A., Lesnick, T.L., Graff-Radford, J., Machulda, M.M., Knopman, D.S., Schwarz, C.G., Lowe, V.J., Mielke, M.M., Petersen, R.C., Jack, C.R., Vemuri, P., 2019. The metabolic brain signature of cognitive resilience in the 80+: beyond Alzheimer pathologies. Brain 142 (4), 1134–1147. https://doi.org/10.1093/brain/awz037.

Atlante, A., de Bari, L., Bobba, A., Amadoro, G., 2017. A disease with a sweet tooth: exploring the Warburg effect in Alzheimer's disease. Biogerontology 18 (3), 301–319. https://doi.org/10.1007/s10522-017-9692-x.

Badhwar, AmanPreet, Tam, A., Dansereau, C., Orban, P., Hoffstaedter, F., Bellec, P., 2017. Resting-state network dysfunction in Alzheimer's disease: A systematic review and meta-analysis. Alzheimers Dement (Amst) 8 (1), 73–85. https://doi.org/10.1016/j.dadm.2017.03.007.

Balthazar, M.L.F., Pereira, F.R.S., Lopes, T.M., da Silva, E.L., Coan, A.C., Campos, B.M., Duncan, N.W., Stella, F., Northoff, G., Damasceno, B.P., Cendes, F., 2014. Neuropsychiatric symptoms in Alzheimer's disease are related to functional connectivity alterations in the salience network. Hum. Brain Mapp. 35 (4), 1237–1246. https://doi.org/10.1002/hbm.22248.

Benson, D.F., Kuhl, D.E., Hawkins, R.A., Phelps, M.E., Cummings, J.L., Tsai, S.Y., 1983. The fluorodeoxyglucose 18F scan in Alzheimer's disease and multi-infarct dementia. Arch. Neurol. 40 (12), 711–714. https://doi.org/10.1001/archneur.1983.04050110029003.

Brier, M.R., Thomas, J.B., Fagan, A.M., Hassenstab, J., Holtzman, D.M., Benzinger, T.L., Morris, J.C., Ances, B.M., 2014. Functional connectivity and graph theory in preclinical Alzheimer's disease. Neurobiol. Aging 35 (4), 757–768. https://doi.org/10.1016/j.neurobiolaging.2013.10.081.

Brier, M.R., Thomas, J.B., Snyder, A.Z., Benzinger, T.L., Zhang, D., Raichle, M.E., Holtzman, D.M., Morris, J.C., Ances, B.M., 2012. Loss of intranetwork and internetwork resting state functional connections with Alzheimer's disease progression. J. Neurosci. 32 (26), 8890–8899.

Bullmore, E.d., Sporns, O., 2012. The economy of brain network organization. Nat. Rev. Neurosci. 13 (5), 336–349. https://doi.org/10.1038/nrn3214.

Cassady, K.E., Adams, J.N., Chen, X.i., Maass, A., Harrison, T.M., Landau, S., Baker, S., Jagust, W., 2021. Alzheimer's pathology is associated with dedifferentiation of intrinsic functional memory networks in aging. Cereb. Cortex 31 (10), 4781–4793. https://doi.org/10.1093/cercor/bhab122.

Cauda, F., D'Agata, F., Sacco, K., Duca, S., Geminiani, G., Vercelli, A., 2011. Functional connectivity of the insula in the resting brain. Neuroimage 55 (1), 8–23. https://doi.org/10.1016/j.neuroimage.2010.11.049.

Chan, M.Y., Park, D.C., Savalia, N.K., Petersen, S.E., Wig, G.S., 2014. Decreased segregation of brain systems across the healthy adult lifespan. Proc. Natl. Acad. Sci. U.S.A. 111 (46), E4997–E5006. https://doi.org/10.1073/pnas.1415122111.

Chand, G.B., Wu, J., Hajjar, I., Qiu, D., 2017. Interactions of the salience network and its subsystems with the default-mode and the central-executive networks in normal aging and mild cognitive impairment. Brain Connect. 7 (7), 401–412. https://doi.org/10.1089/brain.2017.0509.

Chen, A.C., Oathes, D.J., Chang, C., Bradley, T., Zhou, Z.-W., Williams, L.M., Glover, G. H., Deisseroth, K., Etkin, A., 2013. Causal interactions between fronto-parietal central executive and default-mode networks in humans. Proc. Natl. Acad. Sci. U.S. A. 110 (49), 19944–19949. https://doi.org/10.1073/pnas.1311772110.

Chen, Z., Jamadar, S.D., Li, S., Sforazzini, F., Baran, J., Ferris, N., Shah, N.J., Egan, G.F., 2018. From simultaneous to synergistic MR-PET brain imaging: A review of hybrid MR-PET imaging methodologies. Hum. Brain Mapp. 39 (12), 5126–5144. https://doi.org/10.1002/hbm.24314.

Contreras, J.A., Avena-Koenigsberger, A., Risacher, S.L., West, J.D., Tallman, E., McDonald, B.C., Farlow, M.R., Apostolova, L.G., Goñi, J., Dzemidzic, M., Wu, Y.-C., Kessler, D., Jeub, L., Fortunato, S., Saykin, A.J., Sporns, O., 2019. Resting state network modularity along the prodromal late onset Alzheimer's disease continuum. Neuroimage Clin. 22, 101687. https://doi.org/10.1016/j.nicl.2019.101687.

Costumero, V., d'Oleire Uquillas, F., Diez, I., Andorrà, M., Basaia, S., Bueicheků, E., Ortiz-Terán, L., Belloch, V., Escudero, J., Ávila, C., Sepulcre, J., 2020. Distance disintegration delineates the brain connectivity failure of Alzheimer's disease. Neurobiol. Aging 88, 51–60. https://doi.org/10.1016/j.neurobiolaging.2019.12.005.

Cox, R.W., 1996. AFNI: software for analysis and visualization of functional magnetic resonance neuroimages. Comput. Biomed. Res. 29 (3), 162–173. https://doi.org/10.1006/cbmr.1996.0014.

Dai, Z., Lin, Q., Li, T., Wang, X., Yuan, H., Yu, X., He, Y., Wang, H., 2019. Disrupted structural and functional brain networks in Alzheimer's disease. Neurobiol. Aging 75, 71–82. https://doi.org/10.1016/j.neurobiolaging.2018.11.005.

Dai, Z., Yan, C., Li, K., Wang, Z., Wang, J., Cao, M., Lin, Q., Shu, N.i., Xia, M., Bi, Y., He, Y., 2015. Identifying and mapping connectivity patterns of brain network hubs in Alzheimer's disease. Cereb. Cortex 25 (10), 3723–3742. https://doi.org/10.1093/cercor/bhu246.

Del Sole, A., Clerici, F., Chiti, A., Lecchi, M., Mariani, C., Maggiore, L., Mosconi, L., Lucignani, G., 2008. Individual cerebral metabolic deficits in Alzheimer's disease and amnestic mild cognitive impairment: an FDG PET study. Eur. J. Nucl. Med. Mol. Imaging 35 (7), 1357–1366. https://doi.org/10.1007/s00259-008-0773-6.

Egner, T., 2009. Prefrontal cortex and cognitive control: motivating functional hierarchies. Nat. Neurosci. 12 (7), 821–822. https://doi.org/10.1038/nn0709-821.

Ewers, M., Luan, Y., Frontzkowski, L., Neitzel, J., Rubinski, A., Dichgans, M., Hassenstab, J., Gordon, B.A., Chhatwal, J.P., Levin, J., Schofield, P., Benzinger, T.L. S., Morris, J.C., Goate, A., Karch, C.M., Fagan, A.M., McDade, E., Allegri, R., Berman, S., Chui, H., Cruchaga, C., Farlow, M., Graff-Radford, N., Jucker, M., Lee, J.-H., Martins, R.N., Mori, H., Perrin, R., Xiong, C., Rossor, M., Fox, N.C., O'Connor, A., Salloway, S., Danek, A., Buerger, K., Bateman, R.J., Habeck, C., Stern, Y., Franzmeier, N., 2021. Segregation of functional networks is associated with cognitive resilience in Alzheimer's disease. Brain 144 (7), 2176–2185. https://doi.org/10.1093/brain/awab112.

Folstein, M.F., Folstein, S.E., McHugh, P.R., 1975. "Mini-mental state". A practical method for grading the cognitive state of patients for the clinician. J. Psychiatr. Res. 12 (3), 189–198. https://doi.org/10.1016/0022-3956(75)90026-6.

Franzmeier, N., Duering, M., Weiner, M., Dichgans, M., Ewers, M., 2017. Left frontal cortex connectivity underlies cognitive reserve in prodromal Alzheimer disease. Neurology 88 (11), 1054–1061.

Gonzalez-Escamilla, G., Lange, C., Teipel, S., Buchert, R., Grothe, M.J., 2017. PETPVE12: an SPM toolbox for Partial Volume Effects correction in brain PET - Application to amyloid imaging with AV45-PET. NeuroImage 147, 669–677. https://doi.org/10.1016/j.neuroimage.2016.12.077.

Gratton, C., Nomura, E.M., Pérez, F., D'Esposito, M., 2012. Focal brain lesions to critical locations cause widespread disruption of the modular organization of the brain. J. Cogn. Neurosci. 24 (6), 1275–1285. https://doi.org/10.1162/jocn_a_00222.

Greicius, M.D., Srivastava, G., Reiss, A.L., Menon, V., 2004. Default-mode network activity distinguishes Alzheimer's disease from healthy aging: evidence from functional MRI. Proc. Natl. Acad. Sci. U.S.A. 101 (13), 4637–4642. https://doi.org/10.1073/pnas.0308627101.

Harrison, B.J., Pujol, J., Ortiz, H., Fornito, A., Pantelis, C., Yücel, M., Robertson, E., 2008. Modulation of brain resting-state networks by sad mood induction. PLoS ONE 3 (3), e1794. https://doi.org/10.1371/journal.pone.0001794.

He, X., Qin, W., Liu, Y., Zhang, X., Duan, Y., Song, J., Li, K., Jiang, T., Yu, C., 2014. Abnormal salience network in normal aging and in amnestic mild cognitive impairment and Alzheimer's disease. Hum. Brain Mapp. 35 (7), 3446–3464. https://doi.org/10.1002/hbm.22414.

Heiss, W.-D., 2016. Hybrid PET/MR imaging in neurology: present applications and prospects for the future. J. Nucl. Med. 57 (7), 993–995. https://doi.org/10.2967/jnumed.116.175208.

Herholz, K., Carter, S.F., Jones, M., 2007. Positron emission tomography imaging in dementia. Br. J. Radiol. 80 (special_issue_2), S160–S167. https://doi.org/10.1259/bjr/97295129.

Jamadar, S.D., Ward, P.G.D., Liang, E.X., Orchard, E.R., Chen, Z., Egan, G.F., 2021. Metabolic and hemodynamic resting-state connectivity of the human brain: A high-temporal resolution simultaneous BOLD-fMRI and FDG-fPET multimodality study. Cereb. Cortex 31 (6), 2855–2867. https://doi.org/10.1093/cercor/bhaa393.

Jones, D.T., Knopman, D.S., Gunter, J.L., Graff-Radford, J., Vemuri, P., Boeve, B.F., Petersen, R.C., Weiner, M.W., Jack, C.R., 2016. Cascading network failure across the Alzheimer's disease spectrum. Brain 139 (2), 547–562. https://doi.org/10.1093/brain/awv338.

Koesters, T., Friedman, K.P., Fenchel, M., Zhan, Y., Hermosillo, G., Babb, J., Jelescu, I.O., Faul, D., Boada, F.E., Shepherd, T.M., 2016. Dixon sequence with superimposed model-based bone compartment provides highly accurate PET/MR attenuation correction of the brain. J. Nucl. Med. 57 (6), 918–924. https://doi.org/10.2967/jnumed.115.166967.

Li, C., Li, Y., Zheng, L., Zhu, X., Shao, B., Fan, G., Liu, T., Wang, J., 2019. Abnormal brain network connectivity in a triple-network model of Alzheimer's disease. J. Alzheimers Dis. 69 (1), 237–252.

Liang, X., He, Y., Salmeron, B.J., Gu, H., Stein, E.A., Yang, Y., 2015. Interactions between the salience and default-mode networks are disrupted in cocaine addiction. J. Neurosci. 35 (21), 8081–8090.

Liang, X., Zou, Q., He, Y., Yang, Y., 2013. Coupling of functional connectivity and regional cerebral blood flow reveals a physiological basis for network hubs of the human brain. Proc. Natl. Acad. Sci. U.S.A. 110 (5), 1929–1934. https://doi.org/10.1073/pnas.1214900110.

Lim, H.K., Nebes, R., Snitz, B., Cohen, A., Mathis, C., Price, J., Weissfeld, L., Klunk, W., Aizenstein, H.J., 2014. Regional amyloid burden and intrinsic connectivity networks in cognitively normal elderly subjects. Brain 137 (12), 3327–3338. https://doi.org/10.1093/brain/awu271.

Liu, J., Zhu, Y.-S., Khan, M.A., Brunk, E., Martin-Cook, K., Weiner, M.F., Cullum, C.M., Lu, H., Levine, B.D., Diaz-Arrastia, R., Zhang, R., 2014. Global brain hypoperfusion and oxygenation in amnestic mild cognitive impairment. Alzheimers Dement 10 (2), 162–170. https://doi.org/10.1016/j.jalz.2013.04.507.

Manza, P., Wiers, C.E., Shokri-Kojori, E., Kroll, D., Feldman, D., Schwandt, M., Wang, G.-J., Tomasi, D., Volkow, N.D., 2020. Brain network segregation and glucose energy

utilization: relevance for age-related differences in cognitive function. Cereb. Cortex 30 (11), 5930–5942. https://doi.org/10.1093/cercor/bhaa167.
Marchitelli, R., Aiello, M., Cachia, A., Quarantelli, M., Cavaliere, C., Postiglione, A., Tedeschi, G., Montella, P., Milan, G., Salvatore, M., Salvatore, E., Baron, J.C., Pappatà, S., 2018. Simultaneous resting-state FDG-PET/fMRI in Alzheimer disease: relationship between glucose metabolism and intrinsic activity. Neuroimage 176, 246–258. https://doi.org/10.1016/j.neuroimage.2018.04.048.
McKhann, G.M., Knopman, D.S., Chertkow, H., Hyman, B.T., Jack, C.R., Kawas, C.H., Klunk, W.E., Koroshetz, W.J., Manly, J.J., Mayeux, R., Mohs, R.C., Morris, J.C., Rossor, M.N., Scheltens, P., Carrillo, M.C., Thies, B., Weintraub, S., Phelps, C.H., 2011. The diagnosis of dementia due to Alzheimer's disease: recommendations from the National Institute on Aging-Alzheimer's Association workgroups on diagnostic guidelines for Alzheimer's disease. Alzheimers Dement 7 (3), 263–269. https://doi.org/10.1016/j.jalz.2011.03.005.
Menon, V., 2011. Large-scale brain networks and psychopathology: a unifying triple network model. Trends Cogn. Sci. 15 (10), 483–506. https://doi.org/10.1016/j.tics.2011.08.003.
Minoshima, S., Giordani, B., Berent, S., Frey, K.A., Foster, N.L., Kuhl, D.E., 1997. Metabolic reduction in the posterior cingulate cortex in very early Alzheimer's disease. Ann. Neurol. 42 (1), 85–94. https://doi.org/10.1002/ana.410420114.
Morris, J.C., 1993. The clinical dementia rating (CDR): current version and scoring rules. Neurology 43 (11), 2412.2.
Müller-Gärtner, H.W., Links, J.M., Prince, J.L., Bryan, R.N., McVeigh, E., Leal, J.P., Davatzikos, C., Frost, J.J., 1992. Measurement of radiotracer concentration in brain gray matter using positron emission tomography: MRI-based correction for partial volume effects. J. Cereb. Blood Flow Metab. 12 (4), 571–583. https://doi.org/10.1038/jcbfm.1992.81.
Mutlu, J., Landeau, B., Gaubert, M., de La Sayette, V., Desgranges, B., Chételat, G., 2017. Distinct influence of specific versus global connectivity on the different Alzheimer's disease biomarkers. Brain 140 (12), 3317–3328. https://doi.org/10.1093/brain/awx279.
Myers, N., Pasquini, L., Göttler, J., Grimmer, T., Koch, K., Ortner, M., Neitzel, J., Mühlau, M., Förster, S., Kurz, A., Förstl, H., Zimmer, C., Wohlschläger, A.M., Riedl, V., Drzezga, A., Sorg, C., 2014. Within-patient correspondence of amyloid-β and intrinsic network connectivity in Alzheimer's disease. Brain 137 (7), 2052–2064. https://doi.org/10.1093/brain/awu103.
Newman, M.E., Girvan, M., 2004. Finding and evaluating community structure in networks. Phys. Rev. E: Stat. Nonlinear Soft Matter Phys. 69, 026113 https://doi.org/10.1103/PhysRevE.69.026113.
Ng, A.S.L., Wang, J., Ng, K.K., Chong, J.S.X., Qian, X., Lim, J.K.W., Tan, Y.J., Yong, A.C. W., Chander, R.J., Hameed, S., Ting, S.K.S., Kandiah, N., Zhou, J.H., 2021. Distinct network topology in Alzheimer's disease and behavioral variant frontotemporal dementia. Alzheimers Res. Ther. 13 (1) https://doi.org/10.1186/s13195-020-00752-w.
Onoda, K., Ishihara, M., Yamaguchi, S., 2012. Decreased functional connectivity by aging is associated with cognitive decline. J. Cogn. Neurosci. 24 (11), 2186–2198. https://doi.org/10.1162/jocn_a_00269.
Passow, S., Specht, K., Adamsen, T.C., Biermann, M., Brekke, N., Craven, A.R., Ersland, L., Grüner, R., Kleven-Madsen, N., Kvernenes, O.-H., Schwarzlmüller, T., Olesen, R.A., Hugdahl, K., 2015. Default-mode network functional connectivity is closely related to metabolic activity. Hum. Brain Mapp. 36 (6), 2027–2038. https://doi.org/10.1002/hbm.22753.
Power, J.D., Barnes, K.A., Snyder, A.Z., Schlaggar, B.L., Petersen, S.E., 2012. Spurious but systematic correlations in functional connectivity MRI networks arise from subject motion. Neuroimage 59 (3), 2142–2154. https://doi.org/10.1016/j.neuroimage.2011.10.018.
Riedl, V., Bienkowska, K., Strobel, C., Tahmasian, M., Grimmer, T., Forster, S., Friston, K. J., Sorg, C., Drzezga, A., 2014. Local activity determines functional connectivity in the resting human brain: a simultaneous FDG-PET/fMRI study. J. Neurosci. 34 (18), 6260–6266. https://doi.org/10.1523/JNEUROSCI.0492-14.2014.
Ripp, I., Stadhouders, T., Savio, A., Goldhardt, O., Cabello, J., Calhoun, V., Riedl, V., Hedderich, D., Diehl-Schmid, J., Grimmer, T., Yakushev, I., 2020. Integrity of neurocognitive networks in dementing disorders as measured with simultaneous PET/functional MRI. J. Nucl. Med. 61 (9), 1341–1347. https://doi.org/10.2967/jnumed.119.234930.
Rosvall, M., Bergstrom, C.T., 2008. Maps of random walks on complex networks reveal community structure. Proc. Natl. Acad. Sci. U.S.A. 105 (4), 1118–1123. https://doi.org/10.1073/pnas.0706851105.
Scherr, M., Utz, L., Tahmasian, M., Pasquini, L., Grothe, M.J., Rauschecker, J.P., Grimmer, T., Drzezga, A., Sorg, C., Riedl, V., 2021. Effective connectivity in the default mode network is distinctively disrupted in Alzheimer's disease-A simultaneous resting-state FDG-PET/fMRI study. Hum. Brain Mapp. 42 (13), 4134–4143. https://doi.org/10.1002/hbm.24517.
Shokri-Kojori, E., Tomasi, D., Alipanahi, B., Wiers, C.E., Wang, G.-J., Volkow, N.D., 2019. Correspondence between cerebral glucose metabolism and BOLD reveals relative power and cost in human brain. Nat. Commun. 10 (1) https://doi.org/10.1038/s41467-019-08546-x.
Sridharan, D., Levitin, D.J., Menon, V., 2008. A critical role for the right fronto-insular cortex in switching between central-executive and default-mode networks. Proc. Natl. Acad. Sci. U.S.A. 105 (34), 12569–12574. https://doi.org/10.1073/pnas.0800005105.
Tomasi, D., Wang, G.-J., Volkow, N.D., 2013. Energetic cost of brain functional connectivity. Proc. Natl. Acad. Sci. U.S.A. 110 (33), 13642–13647. https://doi.org/10.1073/pnas.1303346110.
Tumati, S., Marsman, J.-B., De Deyn, P.P., Martens, S., Aleman, A., 2020. Functional network topology associated with apathy in Alzheimer's disease. J. Affect. Disord. 266, 473–481. https://doi.org/10.1016/j.jad.2020.01.158.
Waites, A.B., Stanislavsky, A., Abbott, D.F., Jackson, G.D., 2005. Effect of prior cognitive state on resting state networks measured with functional connectivity. Hum. Brain Mapp. 24 (1), 59–68. https://doi.org/10.1002/hbm.20069.
Wig, G.S., 2017. Segregated systems of human brain networks. Trends Cogn. Sci. 21 (12), 981–996. https://doi.org/10.1016/j.tics.2017.09.006.
Zhang, M., Sun, W., Guan, Z., Hu, J., Li, B., Ye, G., Meng, H., Huang, X., Lin, X., Wang, J., Liu, J., Li, B., Zhang, Y., Li, Y., 2021a. Simultaneous PET/fMRI detects distinctive alterations in functional connectivity and glucose metabolism of precuneus subregions in Alzheimer's disease. Front. Aging Neurosci. 13 https://doi.org/10.3389/fnagi.2021.737002.
Zhang, Y., Du, W., Yin, Y., Li, H., Liu, Z., Yang, Y., Han, Y., Gao, J.-H., 2021b. Impaired cerebral vascular and metabolic responses to parametric N-back tasks in subjective cognitive decline. J. Cereb. Blood Flow Metab. 41 (10), 2743–2755. https://doi.org/10.1177/0271678X211012153.
Zhao, Q., Sang, X., Metmer, H., Swati, Z.N.N.K., Lu, J., 2019. Functional segregation of executive control network and frontoparietal network in Alzheimer's disease. Cortex 120, 36–48. https://doi.org/10.1016/j.cortex.2019.04.026.
Zhou, J., Greicius, M.D., Gennatas, E.D., Growdon, M.E., Jang, J.Y., Rabinovici, G.D., Kramer, J.H., Weiner, M., Miller, B.L., Seeley, W.W., 2010. Divergent network connectivity changes in behavioural variant frontotemporal dementia and Alzheimer's disease. Brain 133 (5), 1352–1367. https://doi.org/10.1093/brain/awq075.